Atmos. Chem. Phys. Discuss., 9, 23623–23664, 2009
www.atmos-chem-phys-discuss.net/9/23623/2009/

Atmospheric Chemistry and Physics Discussions

This discussion paper is/has been under review for the journal Atmospheric Chemistry and Physics (ACP). Please refer to the corresponding final paper in ACP if available.

Finding the missing stratospheric Br_y: a global modeling study of $CHBr_3$ and CH_2Br_2

Q. Liang[1,2], R. S. Stolarski[1], S. R. Kawa[1], J. E. Nielsen[3,4], J. M. Rodriguez[1], A. R. Douglass[1], D. R. Blake[5], E. L. Atlas[6], and L. Ott[3,7]

[1]NASA Goddard Space Flight Center, Atmospheric Chemistry and Dynamics Branch, Code 613.3, Greenbelt, MD 20771, USA
[2]Oak Ridge Associated Universities, NASA Postdoctoral Program, Oak Ridge, Tennessee 37831, USA
[3]NASA Goddard Space Flight Center, Global Modeling and Assimilation Office, Code 610.1, Greenbelt, MD 20771, USA
[4]Science Systems and Applications Inc., Lanham, Maryland, USA
[5]University of California, 570 Rowland Hall, Irvine, CA 92697, USA
[6]University of Miami, 4600 Rickenbacker Causeway, Miami, FL 33149, USA

[7]Goddard Earth Sciences and Technology Center, University of Maryland, Baltimore County, Maryland, USA

Received: 2 October 2009 – Accepted: 8 October 2009 – Published: 5 November 2009

Correspondence to: Q. Liang (liangqing@gmail.com)

Published by Copernicus Publications on behalf of the European Geosciences Union.

Abstract

Recent in situ and satellite measurements suggest a contribution of ~5 pptv to stratospheric inorganic bromine from short-lived bromocarbons. We conduct a modeling study of the two most important short-lived bromocarbons, bromoform ($CHBr_3$) and dibromomethane (CH_2Br_2), with the Goddard Earth Observing System Chemistry Climate Model (GEOS CCM) to account for this missing stratospheric bromine. We derive a "top-down" emission estimate of $CHBr_3$ and CH_2Br_2 using airborne measurements in the Pacific and North American troposphere and lower stratosphere (LS) obtained during previous NASA aircraft campaigns. Our emission estimate suggests that to reproduce the observed concentrations in the free troposphere, a global oceanic emission of 425 Gg Br yr^{-1} for $CHBr_3$ and 57 Gg Br yr^{-1} for CH_2Br_2 is needed, with 60% of emissions from open ocean and 40% from coastal regions. Although our simple emission scheme assumes no seasonal variations, the model reproduces the observed seasonal variations of the short-lived bromocarbons with high concentrations in winter and low concentrations in summer. This indicates that the seasonality of short-lived bromocarbons is largely due to seasonality in their chemical loss and transport. The inclusion of $CHBr_3$ and CH_2Br_2 contributes ~5 pptv bromine throughout the stratosphere. Both the source gases and inorganic bromine produced from the source gas degradation (Br_y^{VSLS}) in the troposphere are transported into the stratosphere, and are equally important. Inorganic bromine accounts for half (2.5 pptv) of the bromine from the inclusion of $CHBr_3$ and CH_2Br_2 near the tropical tropopause and its contribution rapidly increases to ~100% as altitude increases. More than 85% of the wet scavenging of Br_y^{VSLS} occurs in large-scale precipitation below 500 hPa and Br_y^{VSLS} in the stratosphere is not sensitive to convection.

ACPD

9, 23623–23664, 2009

1 Introduction

Oceanic emission of very short-lived substances (VSLS) is thought to contribute significantly to reactive bromine in the stratosphere in addition to long-lived halons and methyl bromide (Kurylo and Rodriguez, 1999). VSLS are not accounted for in most chemistry climate models. In the stratosphere, inorganic bromine produced from VSLS (Br_y^{VSLS}) contributes to catalytic destruction of ozone (e.g., McElroy et al., 1986; Solomon et al., 1995; Garcia and Solomon, 1994; Sturges et al., 2000). Br_y^{VSLS} can also have a significant impact on tropospheric ozone (von Glasow et al., 2004; Yang et al., 2005).

A key question is the extent to which VSLS contribute to inorganic bromine (Br_y) in the stratosphere. The difference between ground-based observations of column BrO (Sinnhuber et al., 2002, and references therein) and the fraction of the BrO column which can be accounted for based on long-lived halons and methyl bromide suggests a contribution of ~5 pptv to stratospheric inorganic bromine from VSLS (Sinnhuber et al., 2002). This is consistent with recent balloon-borne measurements which estimated that Br_y^{VSLS} is ~5.2 pptv (Dorf et al., 2008). Br_y^{VSLS} implied from satellite BrO measurements are more variable, ranging from ~3 pptv (Sinnhuber et al., 2005; Livesey et al., 2006) to ~8 pptv (Sioris et al., 2006). The estimated contribution of VSLS to Br_y in the stratosphere also differs in modeling studies. Dvortsov et al. (1999) calculated a maximum of 1.8 pptv Br_y in the stratosphere from bromoform ($CHBr_3$), slightly higher than the 1.1 pptv from Nielsen and Douglass (2001). Warwick et al. (2006) conducted a detailed emission-based modeling analysis of all five major VSL oceanic bromocarbons, including $CHBr_3$, dibromomethane (CH_2Br_2), bromodichloromethane ($CHBrCl_2$), dibromochloromethane ($CHBr_2Cl$), and bromochloromethane (CH_2BrCl). They concluded that very short-lived (VSL) oceanic bromocarbons contribute a maximum of 6–7 pptv Br_y, peaking over the equator at ~100 hPa. Hossaini et al. (2009) estimated that $CHBr_3$ and CH_2Br_2 contribute ~2.4 pptv of inorganic bromine to the lower stratosphere with source gas injection being the dominant pathway.

ACPD
9, 23623–23664, 2009

A large part of the uncertainty in the contribution of VSLS to Br_y in the stratosphere arises from the highly-variable mixing ratios of VSL bromocarbons in the marine boundary layer, ranging from 0.2 pptv to ≫100 pptv (Quack and Wallace, 2003). Therefore, the amount of VSL bromocarbons that enters the free troposphere and stratosphere and its subsequent inorganic bromine may vary depending on the location and timing of emissions. The current estimate of the oceanic emissions of VSL bromocarbons is highly uncertain. Bottom-up emission estimates based on atmospheric and oceanic surface water observations indicate that sea-to-air flux of $CHBr_3$ is between 210–820 Gg Br yr^{-1} (Carpenter and Liss, 2000; Quack and Wallace, 2003; Yokouchi et al., 2005; Butler et al., 2007) and that for CH_2Br_2 ranges between 61–280 Gg Br yr^{-1} (Yokouchi et al., 2005; Butler et al., 2007). Modeling studies that derive top-down emission estimates by reproducing background atmospheric concentrations suggest that global emission of $CHBr_3$ ranges between 190–570 Gg Br yr^{-1} (e.g. Dvortsov et al., 1999; Kurylo and Rodriguez, 1999; Nielsen and Douglass, 2001; Warwick et al., 2006) and that of CH_2Br_2 is between 43–104 Gg Br yr^{-1} (e.g. Dvortsov et al., 1999; Warwick et al., 2006).

In this paper, we use the GEOS Chemistry Climate Model (GEOS CCM) together with aircraft measurements from previous NASA field missions to derive a top-down emission estimate of $CHBr_3$ and CH_2Br_2, the two most important VSL bromocarbons. Together, $CHBr_3$ and CH_2Br_2 account for >80% VSL organic bromine in the marine boundary layer and free troposphere (WMO, 2007). We present a quantitative estimate of their contribution to reactive bromine in the stratosphere with our optimized emission estimate. Compared to many previous studies, this study has two major improvements. First, we derive the top-down emission estimate and evaluate model results with an extensive set of aircraft measurements obtained during eight previous NASA field missions throughout the Pacific/North America region. The broad spatial and temporal coverage of these measurements lends more confidence in the robustness of our derived results. Secondly, unlike all previous modeling studies that assume a constant wash-out lifetime of Br_y of 10-days (Dvortsov et al., 1999; Nielsen and Douglass, 2001;

ACPD
9, 23623–23664, 2009

Warwick et al., 2006; Hossaini et al., 2009), we implement a detailed wet deposition scheme that includes scavenging in convective updrafts and rainout/washout in large-scale precipitation. This is to assure a more realistic representation of the impact of large-scale/convective transport on the highly soluble Br_y.

2 Model

2.1 Description

Model simulations are conducted using the Goddard Space Flight Center (GSFC) GEOS CCM Version 2 (V2), an augmented version of GEOS CCM Version 1 (V1) as described in Pawson et al. (2008). The model has a spatial resolution of 2° latitude by 2.5° longitude and 72 layers extending from the surface to 0.01 hPa. The model couples the GEOS-5 GCM (Reinecker et al., 2008) with an updated version of the stratospheric chemistry module described by Douglass and Kawa (1999). The photochemical scheme includes all important gas phase reactions for the stratosphere (Douglass and Kawa, 1999) and uses the chemical kinetics from JPL 2006. Photolysis rates are calculated using the temperature dependent cross sections from JPL 2006. The model uses a flux-form semi-Lagrangian dynamical core (Lin, 2004). Moist processes in GEOS-5 are represented using a convective parameterization and prognostic cloud scheme. Convection is parameterized using the relaxed Arakawa Schubert (RAS) scheme developed by Moorthi and Suarez (1992) in which the atmosphere is relaxed towards equilibrium. Ott et al. (2009) provide a detailed analysis of the GEOS-5 moist physics scheme and its impact on tracer transport, describing the prognostic cloud scheme and comparing results with observations. The scheme calculates large-scale ice and liquid condensate by assuming a probability distribution function for total water. Condensate is subsequently removed from the model domain by evaporation, auto-conversion of liquid condensate, sedimentation of frozen condensate, and accretion of condensate by falling precipitation. The GEOS-5 GCM produces general pre-

ACPD
9, 23623–23664, 2009

cipitation patterns that correlate well with the Global Precipitation Climatology Project (GPCP) data (r=0.65). The stratospheric and tropospheric transport produced by the GEOS-CCM has been extensively evaluated in many previous studies (e.g. Eyring et al., 2006; Waugh et al., 2007; Pawson et al., 2008; Douglass et al., 2008; Liang et al., 2008). The GEOS CCM simulations agree well with observations in many of the meteorological, transport-related, and chemical diagnostics.

2.2 Bromine chemistry in the GEOS CCM

For this study, we modify the standard stratospheric photochemistry scheme to include simple VSL bromocarbon chemistry. In this simple chemistry scheme, $CHBr_3$ and CH_2Br_2 are destroyed via photolysis and reaction with OH. Photolysis rates are calculated using the JPL 2006 cross sections. Rates of reaction with OH are calculated using temperature-dependent expressions from JPL 2006. OH above the tropopause is calculated online in the stratospheric chemistry module. Below the tropopause, OH is relaxed to zonal-averaged 2-dimentional monthly mean fields archived during a full chemistry simulation from the GEOS-Chem chemistry transport model (Bey et al., 2001). GEOS-Chem includes detailed tropospheric O_3-NO_x-NMHC chemistry and simulated OH compares reasonably well with observations (Bey et al., 2001). The mean tropospheric OH concentration is 11×10^5 molecules cm^{-1} and yields an atmospheric lifetime of 5.1 years for methyl chloroform, within the uncertainty of observational estimates (Bey et al., 2001).

Since >80% of the inorganic bromine produced by the degradation of $CHBr_3$ and CH_2Br_2 (Br_y^{VSLS}) in the troposphere is in the form of hydrobromic acid (HBr) and hypobromous acid (HOBr) and both are highly soluble (Yang et al., 2005), for simplicity, we track the degradation products as a single tracer. Br_y^{VSLS} is "transported as an individual tracer" and subject to wet and dry deposition, but does not interact with standard stratospheric chemistry. We adopt the wet and dry deposition scheme from the Goddard

Chemistry Aerosol Radiation and Transport (GOCART) model (Chin et al., 2000). Wet deposition includes scavenging in convective updrafts and rainout/washout in large-scale precipitation (Giorgi and Chameides, 1986; Balkanski et al., 1993). We assume high solubility and Br_y^{VSLS} is removed completely when convective updrafts or large-scale precipitation is encountered. Dry deposition includes gravitational settling with a uniform deposition velocity of 0.3 cm/s, a simplified value based on Yang et al. (2005).

Figure 1 presents the calculated lifetime of $CHBr_3$ and CH_2Br_2 from the GEOS CCM bromocarbon simulation. The simulated atmospheric lifetime (τ) of $CHBr_3$ is 20 days with photolysis being the dominant sink ($\tau_{h\upsilon}$=27 days, τ_{OH}=81 days), consistent with the lifetime calculated in Warwick et al. (2006) (varying between 15–37 days with the choice of emissions). Degradation of CH_2Br_2 occurs predominantly via reaction with OH ($\tau_{h\upsilon}$=8300 days, τ_{OH}=143 days). The simulated atmospheric lifetime of CH_2Br_2 is 140 days. Local lifetime of VSL bromocarbons is highly variable, from ~15 days for $CHBr_3$ and ~90 days for CH_2Br_2 in the tropics to ~180 days ($CHBr_3$) and ~ 540 days (CH_2Br_2) in the poles, similar to the results in Dvortsov et al. (1999) and Hossaini et al. (2009). Dvortsov et al. (1999) calculated that the tropical tropospheric lifetime of $CHBr_3$ is of the order of 2–3 weeks and that of CH_2Br_2 is 2–3 months. Hossaini et al. (2009) showed that local lifetime of $CHBr_3$ ranges between ~15 days (compared to ~13 days in this work) at the tropical surface to ~25–30 days (30 days this work) in the tropical tropopause layer (TTL), and that of CH_2Br_2 ranges from ~50 days (~70 days this work) at the surface to ~520 days (~540 days this work) in the TTL. Our simulated seasonal cycle of $CHBr_3$ at Hawaii (maximum in winter ~0.7 pptv and minimum in summer ~0.3 pptv) matches well with observations from Atlas and Ridley (1996). This seasonal cycle is generated by transport and chemistry in the lower troposphere (Nielsen and Douglass, 2001), which implies that the model captures well chemical loss and tropospheric transport processes.

The simulated "atmospheric lifetime Br_y" against wet deposition is ~15 days with column-integrated rainout/washout lifetime varying from ~10 days in the tropics to ~2 months at high latitudes. The calculated lifetime of Br_y^{VSLS} against dry deposition

ACPD
9, 23623–23664, 2009

is greater than 20 years, suggesting surface dry deposition is of negligible importance compared with wet scavenging.

3 Emission scenarios

In this work, we derive a "top-down" emission scenario (scenario A) of $CHBr_3$ and CH_2Br_2 using observations from previous aircraft campaigns as constraints. We conduct a 12-year GEOS CCM bromine simulation with emission scenario A and examine the chemistry and transport of VSL bromocarbons and their degradation product, Br_y^{VSLS}, in the atmosphere. The simulation is driven by sea surface temperatures (SST) from 1990 to 2001, but otherwise does not correspond to any specific year. We initialized the simulation with zero-concentrations for $CHBr_3$ and CH_2Br_2. For $CHBr_3$ (lifetime ~1 month) and CH_2Br_2 (lifetime of ~4 months) a 3 year simulation length has been used by most previous modeling studies and is generally thought to be adequate. However, transport in the stratosphere is slow and Br_y has no significant loss process in the atmosphere other than removal by wet scavenging in the troposphere, thus a 3 year simulation is not sufficient to quantitatively understand the contribution of VSL bromocarbons to reactive bromine in the stratosphere. Here we extend the simulation length to 12 years to investigate whether the duration of the simulation affects the troposphere-to-stratosphere transport of Br_y.

We conduct two sensitivity simulations with two additional emission scenarios (scenario B and C) from Warwick et al. (2006), which were demonstrated to reproduce well the observed $CHBr_3$ concentrations during the NASA PEM-Tropics mission. For computational efficiency, the two sensitivity simulations are run for three years driven by SST from 1990–1992. Results from year 3 from all three simulations are compared with each other to understand the impact of emission distribution on simulated bromocarbon concentrations.

The details of each scenario are listed in Table 1 and emission distributions are presented in Fig. 2. For simplicity we assume no seasonal variability in emissions in

ACPD
9, 23623–23664, 2009

all three scenarios. We refer to the three simulations as simulation A (with emission scenario A), simulation B (with scenario B), and simulation C (with scenario C).

3.1 Scenario A

We use measurements from eight NASA aircraft missions between 1996 and 2008 as observational constraints. A detailed list of the aircraft missions is presented in Table 2 and geographic distribution of all flight tracks are shown in Fig. 3. The composite of bromocarbon measurements in the troposphere covers the entire Pacific and North America region. Measurements in the upper troposphere/lower stratosphere (UT/LS) are concentrated in the tropics. Whole air samples were collected by stainless steel canisters onboard the NASA DC-8, ER-2, and WB-57F aircrafts and later analyzed using gas chromatography with mass selective detection (GC/MS) (Schauffler et al., 1999; Blake et al., 2003).

We derive the emission distribution of $CHBr_3$ using 10 individual components representing emissions from open ocean and coastlines at 10° S–10° N, 10–50° S/° N, and 50–90° S/° N, respectively (Fig. 2 and Table 1). Within each regional component, emission is uniformly distributed at all surface grid boxes. We determine the magnitude of emission of $CHBr_3$ from each region by simultaneously matching the observed concentration in the middle troposphere and the observed vertical gradient in the corresponding region. Since $CHBr_3$ and CH_2Br_2 are emitted by the same marine macroalgae sources, we employ the same distribution for CH_2Br_2 as that derived for $CHBr_3$. The global emission magnitude for CH_2Br_2 is deduced by matching the simulated concentrations with background atmospheric observations. Our best estimate yields a global emission of 425 Gg Br yr^{-1} for $CHBr_3$, with 255 Gg Br yr^{-1} (60%) and 170 Gg Br yr^{-1} (40%) over the open ocean and along the coastlines, respectively. Our estimate of $CHBr_3$ emission from coastal regions is similar to the bottom-up coastal estimate of 200 Gg Br yr^{-1} from Carpenter et al. (2009). The emission is latitude-dependent, with 160 Gg Br yr^{-1} (~38%) concentrated in a narrow tropical band between 10° S and 10° N, 95 Gg Br yr^{-1} (22%) and 150 Gg Br yr^{-1} (35%) in the Southern and Northern sub-

ACPD
9, 23623–23664, 2009

topics and mid-latitudes between 10° and 50° north and south, respectively. A small amount, 10 Gg Br yr^{-1}, is emitted at the Northern and Southern high latitudes, respectively. The global emission of CH_2Br_2 is estimated to be 57 Gg Br yr^{-1}. Our emission estimates are likely a low limit estimate of the oceanic emission for $CHBr_3$ as the model does not reproduce the very high mixing ratios observed in the marine boundary layer near coastlines.

3.2 Scenario B

This scenario uses the emission distribution of Scenario 3 from Warwick et al. (2006). In this scenario, a total of 380 Gg Br yr^{-1} for $CHBr_3$ and 104 Gg Br yr^{-1} forCH_2Br_2 are emitted at the surface. The emissions are concentrated in the tropical open oceans, with 75% distributed uniformly in the open ocean between 20° S and 20° N and the remaining 25% between 20° and 50° north and south (Fig. 2 and Table 1).

3.3 Scenario C

This is based on Scenario 5 of Warwick et al. (2006). We follow Warwick et al. (2006) and use a global emission of 565 Gg Br yr^{-1} for $CHBr_3$. We reduce the global emission of CH_2Br_2 to 57 Gg Br yr^{-1} to correct the model high bias as compared to observations (Sect. 4). The emission distribution contains a combination of open ocean emissions and tropical coastline emissions, with ~50% emitted in the open ocean between 50° S and 50° N, and the remaining 50% along the tropical coastline between 10° S and 10° N (Fig. 2 and Table 1).

ACPD
9, 23623–23664, 2009

4 Comparison with observations

4.1 $CHBr_3$

We compare the simulated bromocarbons with the composite of aircraft measurements. Figure 4 shows the observed and simulated $CHBr_3$ concentrations in the lower troposphere between 800–1000 hPa. We separate aircraft observations into two periods, February–May and June–October. Since more than 95% of the observations are concentrated between March–May (MAM) and July–September (JAS), we sample the model at the closest grid point in MAM and JAS and compare with observations. The MAM and JAS periods approximate the boreal spring and summer seasons, respectively. Both the observed and simulated $CHBr_3$ are regridded to a horizontal resolution of 10° times 8° for easy comparison.

High $CHBr_3$ concentrations are found in a narrow tropical band between 10° S–10° N as well as along the coasts, in contrast to relatively low values in the northern/southern central pacific and the center of the continents. This spatial distribution is consistent with the short atmospheric lifetime of $CHBr_3$. As a result, high concentrations of $CHBr_3$ are found only in close proximity to the source regions. $CHBr_3$ also shows significant seasonal contrast in concentrations with high values during cold seasons and low values during warm seasons. Despite a simple emission scheme with no seasonality, the model reproduces well the spatial distribution and seasonal variation of $CHBr_3$. The simulated $CHBr_3$ correlates well with the observations (r=0.63). This indicates the seasonal variability of $CHBr_3$ is largely controlled by the seasonality in chemical loss and tropospheric transport (Nielsen and Douglass, 2001). The lower concentrations during warm seasons are due to efficient chemical destruction by photolysis and reaction with OH. Sensitivity simulations show that confining the high open ocean emission between 10° S–10° N is essential in re-creating the high concentration band in the tropics. This is due to the relatively zonal advection in the equatorial Pacific associated with the surface trade winds. If the high emission band were extended further, an abrupt increase in photolysis rates or OH concentration from 10° S–10° N to 10–20° S/° N would

ACPD
9, 23623–23664, 2009

be needed to reproduce the contrast in the observed $CHBr_3$ mixing ratios between 10° S–10° N and 10–20° S/° N, which is unlikely.

Figure 5 shows the latitudinal dependence of $CHBr_3$ at the surface. We average aircraft measurements between 0–1 km for every 10° latitude band. Surface $CHBr_3$ maximizes in the tropics as well as the high latitudes. Minimum $CHBr_3$ concentrations are found at ~30° S/° N. The peak in the tropics is due to high emissions while the peaks at the high latitudes are the result of relatively long lifetime. This latitudinal variation agrees well with that from previous surface measurements listed in Table 2 in Quack and Wallace (2003), which includes all published atmospheric mixing ratios of $CHBr_3$ prior to 2003. The model reproduces relatively well the latitudinal dependence of $CHBr_3$ except an underestimate of ~1 pptv in the Arctic. This model-observation difference is likely a result of under-representation of emission at the ice-water interface, associated with emission from ice algae (Sturges et al., 1992; Sturges et al., 1997), which is difficult to reproduce with a coarse model resolution.

We further compare the simulated vertical profiles of $CHBr_3$ with observations for individual aircraft missions (Fig. 6). We sample the model at the nearest grid point to the measurement location in the corresponding month. Mixing ratio of $CHBr_3$ at the surface is ~1–2 pptv, and decreases rapidly to ~0.6 pptv in the middle troposphere and to <0.4 pptv near 200 hPa. Although regions covered by individual aircraft missions differ greatly from each other and we deploy a simplified zonal-uniform emission scheme, the model in general reproduces reasonably well the observed concentration, variability, and vertical gradient during most of the missions. The overestimate during ARCTAS-A is most likely due to the lack of seasonality in our oceanic emission of VSL bromocarbons. To match both the observed profile from ARCTAS-A (April) and ARCTAS-B (July) would require a seasonal-varying emission in the high latitudes with about zero emission in winter and a peak in summer. This seasonality agrees well with several previous studies, suggesting that $CHBr_3$ released from macroalgae maximizes in summer due to enhanced tissue decay and light stimulation (e.g. Goodwin et al., 1997; Klick et al. 1993; Carpenter et al., 2000).

ACPD
9, 23623–23664, 2009

The model does not capture the vertical gradient or variability of $CHBr_3$ observed during the INTEX-B Texas deployment. Significant forest fire plumes were sampled during INTEX-B (Singh et al., 2009). A close examination of trace gas measurements along flight tracks shows that high $CHBr_3$ mixing ratios are coincident with high levels of tracers for biomass burning, e.g. carbon monoxide, hydrogen cyanide and acetonitrile. This suggests that biomass burning is a possible additional source of $CHBr_3$. High mixing ratios of $CHBr_3$ associated with African savannah biomass burning plumes were documented in Carpenter et al. (2007). The lack of biomass burning emission can also explain the lack of variability in simulated $CHBr_3$ mixing ratios compared with the high variability observed in the INTEX-A mission, during which significant biomass burning plumes were sampled (Turquety et al., 2007; Liang et al., 2007).

Observed $CHBr_3$ concentrations in the UT/LS during recent missions, Pre-AVE, AVE, and TC4 (0.2–0.3 pptv), are significantly higher than that measured in 1996 during the early STRAT mission (<0.1 pptv) (Fig. 7). Aircraft and balloon-borne measurements of $CHBr_3$ in the lower stratosphere obtained in 1997 also show $CHBr_3$ mixing ratios less than 0.1 pptv above 12 km (Sturges et al., 2000). However, long-term observations at the surface display little interannual variability in $CHBr_3$ concentrations (WMO, 2007). This implies that this increase in $CHBr_3$ mixing ratios in the lower stratosphere from the mid 1990's to the mid 2000's is possibly due to interannual variations in atmospheric loss process and/or troposphere-to-stratospheric transport. The GEOS CCM reproduces well the observed $CHBr_3$ concentrations in the UT/LS when compared against measurements obtained during Pre-AVE, AVE, and TC4 field missions (Fig. 7), suggesting a good representation of the atmospheric losses and troposphere-to-stratosphere transport of $CHBr_3$ in the UT/LS in the GEOS CCM. The model fails to produce the very low concentrations observed during STRAT between 100–200 hPa. A similar problem was identified by Dvortsov et al. (1999) and Nielsen and Douglass (2001). Both attribute this model-observation difference to excessive convective transport from the boundary layer to the upper troposphere. The fact that GEOS CCM captures well the observed profiles during Pre-AVE, AVE, and TC4 implies

ACPD
9, 23623–23664, 2009

that the overestimate during STRAT may not be due to excessive convective transport. A better understanding of the cause of this overestimate during STRAT is beyond the scope of this paper.

4.2 CH_2Br_2

Due to its longer lifetime, CH_2Br_2 shows less variability in its atmospheric concentration compared to $CHBr_3$. This is clearly seen in lower tropospheric distribution (Fig. 8) as well as vertical profile (Figs. 9 and 10) observed during previous aircraft missions. Annual mean mixing ratios of CH_2Br_2 are ~1 pptv throughout the troposphere with weak vertical gradients near the surface (Fig. 9). The mean mixing ratio of CH_2Br_2 is ~0.5 pptv near the tropical tropopause (Fig. 10). Most of the variability in the troposphere is tied to the seasonality in lifetime due to higher rates of reaction with OH in warmer seasons.

The model reproduces well the observed horizontal distribution of CH_2Br_2 in the lower troposphere (Fig. 8, r=0.78) as well as the vertical gradient in the free troposphere and UT/LS. Sensitivity simulations show that, unlike $CHBr_3$, CH_2Br_2 is not sensitive to details in the open ocean vs. coastal proportion in emission distribution. This is consistent with the fact that CH_2Br_2 has a relatively long lifetime and is more uniformly mixed. Yet its lifetime is short enough to differentiate emissions between tropics, middle latitudes, and high latitudes. An accurate latitudinal distribution in emission is important in reproducing the atmospheric concentration and vertical gradient of CH_2Br_2 at the corresponding latitudes. While we did not derive an emission distribution specifically for CH_2Br_2, our simulated CH_2Br_2 and its vertical gradient matches well with observations. This is consistent with the fact that both are emitted from the same ocean macroalgae and their atmospheric concentrations are highly correlated (Yokouchi et al., 2005).

ACPD
9, 23623–23664, 2009

4.3 Impact of emission

In this section, we examine the impact of differences in emission on atmospheric concentrations of $CHBr_3$ and CH_2Br_2.

Figure 11 compares the annual mean $CHBr_3$ from year 3 of simulations A, B, and C. Simulations B and C reproduce relatively well the observed high concentration band in the tropics, but the band ($CHBr_3$>1 pptv) is too wide compared to observations due to reasons discussed above (Sect. 3). The simulated concentrations at the mid and high latitudes are significantly lower than that from simulation A. This inadequacy in the latitudinal gradient of $CHBr_3$ is also apparent when compared to surface measurements (Fig. 5). Simulations B and C also have difficulty in reproducing the vertical gradient of $CHBr_3$ for aircraft missions that took place at the middle and high latitudes (Fig. 6). These simulation biases are due to an underestimate in oceanic emission at the corresponding latitudes. Sensitivity simulations show that as a result of its short lifetime, the influence of surface $CHBr_3$ emissions does not extend far, either horizontally or vertically. To reproduce the observed vertical profile, it is necessary to have oceanic emission underneath or in adjacent regions. The rate that $CHBr_3$ concentration falls off with altitude is sensitive to the emission magnitude, and thus is a useful constraint to derive emission strength in the corresponding region. Interestingly, while all three simulations have quite different emissions, they reproduce well the observed vertical profiles of $CHBr_3$ during PEM-Tropics A and B in the central and southern Pacific (Fig. 6). This is consistent with the results in Warwick et al. (2006), who found both scenarios B and C yield a good match with observations. While the simulated $CHBr_3$ from simulation C agrees well with the tropical open ocean observations obtained during PEM-Tropics, it is too high compared with the troposphere/lower stratosphere measurements obtained during TC4, Pre-Ave, and HAVE2 along the tropical west coast of South America (Figs. 6 and 7). This implies that the 280 Gg Br yr^{-1} tropical coastal emissions used in scenario C is likely too high.

ACPD
9, 23623–23664, 2009

The simulated CH_2Br_2 concentration is sensitive to the magnitude of global emission as well as latitudinal distribution. Simulation B produces much higher CH_2Br_2 concentrations compared with the observations and the other two simulations in most of the troposphere and LS except in the northern high latitudes (Figs. 9 and 10). The global emission of 104 Gg Br yr^{-1} used in simulation B was deduced in Warwick et al. (2006) by matching the background atmospheric concentrations. This number is twice that derived in this study, and the difference is most likely due to differences in the OH fields used by the two models. OH in the atmosphere is controlled by various chemical and moist physical processes and an accurate representation of OH in global chemistry remains an active yet challenging research task. The difference between simulation A and C (Fig. 9) illustrates the sensitivity of atmospheric CH_2Br_2 mixing ratios to emission at the corresponding latitudes. While CH_2Br_2 displays a much weaker vertical gradient compared to $CHBr_3$, its vertical gradient is a useful indicator of surface emissions, similar to $CHBr_3$. With little emissions in the mid and high latitudes (simulation C), it is difficult to reproduce the observed concentrations as well as the vertical gradients.

The above suggests that top-down emission estimate of short-lived bromocarbons are subject to great uncertainties introduced by the abundance of available measurements, both spatially and temporally, and model OH fields. Differences between this study and that from Warwick et al. (2006) suggest that the uncertainty can be as high as 100%. In addition, while observed vertical gradient is a useful constraint in deriving surface emissions as shown by many previous studies, it is helpful to combine vertical profiles with horizontal distributions to achieve an accurate emission estimate globally.

5 The contribution of short-lived bromocarbons to stratospheric bromine

The simulated $CHBr_3$ and CH_2Br_2 concentrations in the troposphere reach steady state in about or less than one year. In contrast, their impact on total bromine levels in the stratosphere, particularly Br_y, approaches steady state much more slowly, a result of slow transport in the stratosphere. Figure 12 shows the temporal increment of total

bromine produced from VSL bromocarbons (Br^{VSLS}) at different locations in the stratosphere. Total bromine near the tropical tropopause (0° N, 100 hPa) reaches steady state concentration at the end of year 2 while bromine near the middle/high latitude tropopause and in the tropical mid/upper stratosphere gradually increases. The entire stratosphere approaches steady state at year 12. The zonal averaged Br^{VSLS} from year 3 of the simulation shows that the troposphere-to-stratosphere transport of Br^{VSLS} occurs via vertical advection into the tropical stratosphere and quasi-horizontal isentropic transport into the mid-latitude lower stratosphere (Fig. 13c), similar to results from Nielsen and Douglass (2001). The middle and high latitude lower stratosphere is controlled by the relatively rapid quasi-horizontal cross-tropopause isentropic transport from the tropical troposphere and the slower descending motion associated with the mean meridional circulation (Nielsen and Douglass, 2001). As a result, Br^{VSLS} in the middle/high latitude lower stratosphere increases rapidly at the beginning of the simulation and approaches steady state more slowly than that at the equatorial middle and high stratosphere (Fig. 12).

Figures 13d–f and 14 present the steady-state contribution of $CHBr_3$ and CH_2Br_2 to bromine in the atmosphere. At steady state, inclusion of $CHBr_3$ and CH_2Br_2 adds a uniform ~5 pptv to total bromine in the entire stratosphere, set by Br^{VSLS} concentration at the entry point – the tropical tropopause layer. Previous modeling studies with 3–4 years of simulation length suggested that contribution of very short-lived bromocarbons to inorganic bromine in the stratosphere peaks at a certain altitude in the stratosphere (e.g. Nielsen and Douglass, 2001; Warwick et al., 2006). However, our results demonstrate that this is merely a snap-shot contribution amid the spin-up process. As we can clearly seen in Fig. 13b, at year 3, Br_y^{VSLS} peaks in the tropical lower stratosphere. As the simulation continues, the maximum Br_y^{VSLS} area extends further both horizontally and vertically until reaching steady state concentration throughout the entire stratosphere.

ACPD
9, 23623–23664, 2009

Troposphere-to-stratosphere transport of source gases and their degradation products are equally important. Inorganic bromine accounts for half of Br^{VSLS} near the tropopause and its contribution increases rapidly with altitude as source gases quickly photo-dissociates to produce Br_y. Above 50 hPa, almost all is in the form of Br_y. The contribution of CH_2Br_2 to reactive bromine in the stratosphere is of equal or greater importance as that of $CHBr_3$. While $CHBr_3$ contributes mostly via product gas injection, source gas injection is a more important pathway for CH_2Br_2.

About 30% of the Br_y produced from $CHBr_3$ and CH_2Br_2 in the troposphere is removed by wet scavenging, and more than 85% of the wet removal is due to large-scale precipitation below 500 hPa. The mixing ratio of Br^{VSLS} is relatively constant from the tropical middle troposphere to the stratopause, implying little wet scavenging during troposphere-to-stratosphere transport. We conducted a 12-year sensitivity simulation without wet scavenging in convective updrafts and found that convective removal only accounts for ~0.2 pptv (4%) difference in Br_y^{VSLS} in the stratosphere, contrary to the conventional wisdom. This result agrees with the sensitivity study of Dvortsov et al. (1999), who found that estimates of Br_y in the lowermost stratosphere are not very sensitive to convection. A more recent study by Hossaini et al. (2009) also suggests that direct injection of $CHBr_3$ and CH_2Br_2 into the stratosphere is not very sensitive to model parameterized convection.

6 Conclusions

We performed a modeling study using the GEOS CCM to quantify the contribution of $CHBr_3$ and CH_2Br_2 to reactive bromine in the stratosphere. We conducted a 12-year bromocarbon simulation which includes a detailed representation of oceanic emissions of $CHBr_3$ and CH_2Br_2, their chemical losses through photolysis and reaction with OH, surface dry deposition of inorganic bromine (their degradation product), and wet scavenging of inorganic bromine in large-scale precipitation and convective updrafts.

ACPD
9, 23623–23664, 2009

We used observed concentrations and vertical profiles of $CHBr_3$ and CH_2Br_2 from previous NASA aircraft campaigns, including PEM-tropics, TRACE-P, INTEX, ARCTAS, TC4, STRAT, Pre-AVE and AVE, to derive a top-down emission estimate of $CHBr_3$ and CH_2Br_2 from oceanic sources. To produce the observed background mixing ratios, we estimated that the global emissions of $CHBr_3$ and CH_2Br_2 are 425 Gg Br yr^{-1} and 57 Gg Br yr^{-1}, respectively, with 60% from open ocean and 40% from coastlines. Our emission estimates agree well with previous modeling estimates and are within the uncertainty range of bottom-up emission estimates. The 425 Gg Br yr^{-1} for $CHBr_3$ is likely a lower limit as the model does not reproduce the very high mixing ratios observed in the marine boundary layer. Our sensitivity simulations indicate that top-down emission estimate for CH_2Br_2 is sensitive to the model representation of atmospheric OH concentration as reaction with OH is the dominant process for degradation of CH_2Br_2.

When initialized with zero atmospheric concentrations, the transport of bromocarbon source gases and the resulted inorganic bromine to the stratosphere approach steady state in ~12 years. At steady state, including $CHBr_3$ and CH_2Br_2 adds a ubiquitous ~5 pptv to total bromine in the stratosphere, with transport of source gases and transport of their degradation product being equally important. Inorganic bromine accounts for a half (~2.5 pptv) of total bromine from the VSL bromocarbons near the tropopause. Its contribution increases rapidly with altitude and reaches a constant ~5 pptv at 50 hPa and above.

Bromoform has been suggested to play the most important role among short-lived oceanic bromocarbons in contributing reactive bromine to the stratosphere. Our results indicate that CH_2Br_2 is of equal or greater importance. While $CHBr_3$ contributes mostly via product gas injection, source gas injection is a more important pathway for CH_2Br_2.

More than 85% of the wet scavenging of Br_y^{VSLS} occurs below 500 hPa due to large-scale precipitation. Great emphasis has been placed on the impact of convective transport on the troposphere-to-stratosphere transport of VSL bromocarbons and wet scavenging of the resulted inorganic bromine. However, our sensitivity study shows that convective scavenging only accounts for ~0.2 pptv (4%) difference in inorganic bromine

ACPD
9, 23623–23664, 2009

delivered to the stratosphere, assuming 100% removal when convective updraft is encountered.

Acknowledgements. This research was supported by an appointment to the NASA Postdoctoral Program at the Goddard Space Flight Center, administered by Oak Ridge Associated Universities through a contract with NASA.

References

Atlas, E. L. and Ridley, B. A.: The Mauna Loa Observatory Photochemistry Experiment: Introduction, J. Geophys. Res., 101, 14531–14541, 1996.

Balkanski, Y. J., Jacob, D. J., Gardner, G. M., Graustein, W. C., and Turekian, K. K.: Transport and residence times of tropospheric aerosols inferred from a global three-dimensional simulation of ^{210}Pb, J. Geophys. Res., 98, 20573–20586, 1993.

Bey, I., Jacob, D. J., Yantosca, R. M., Logan, J. A., Field, B. D., Fiore, A. M., Li, Q., Liu, H. Y., Mickley, L. J., and Schultz, M. G.: Global modeling of tropospheric chemistry with assimilated meteorology: Model description and evaluation, J. Geophys. Res., 106, 23073–23096, 2001.

Blake, N. J., Blake, D. R., Simpson, I. J., et al.: NMHCs and halocarbons in Asian continental outflow during TRACE-P: Comparison to PEM-WestB, J. Geophys. Res., 108(D20), 8806, doi:10.1029/2002JD003367, 2003.

Butler, J. H., King, D. B., Montzka, S. A., Lobert, J. M., Yvon-Lewis, S. A., and Warwick, N. J.: Oceanic fluxes of CHBr3, CH2Br2, and CH3I into the marine boundarylayer, Global Biogeochem. Cy., 21, GB1023, doi:10.1029/2006GB002732, 2007.

Carpenter, L. J. and Liss, P. S.: On temperate sources of Bromoform and other reactive organic bromine gases, J. Geophys. Res., 105(D16), 20539–20547, 2000.

Carpenter, L. J., Malin, G., Kuepper, F., and Liss, P. S.: Novel biogenic iodine-containing trihalomethanes and other short-lived halocarbons in the coastal East Atlantic, Global Biogeochem. Cy., 14, 1191–1204, 2000.

Carpenter, L. J., Wevill, D. J., Hopkins, J. R., Dunk, R. M., Jones, C. E., Hornsby, K. E., and McQuaid, J. B.: Bromoform in tropical Atlantic air from 25° N to 25° S, Geophys. Res. Lett., 34, L11810, doi:10.1029/2007GL029893, 2007.

Carpenter, L. J., Jones, C. E., Dunk, R. M., Hornsby, K. E., and Woeltjen, J.: Air-sea fluxes of biogenic bromine from the tropical and North Atlantic Ocean, Atmos. Chem. Phys., 9, 1805–1816, 2009, http://www.atmos-chem-phys.net/9/1805/2009/.

Chin, M., Rood, R. B., Lin, S.-J., Muller, J. F., and Thompson, A. M.: Atmosphericsulfur cycle in the global model GOCART: Model description and global properties, J. Geophys. Res., 105, 24671–24687, 2000.

Dorf, M., Butz, A., Camy-Peyret, C., Chipperfield, M. P., Kritten, L., and Pfeilsticker, K.: Bromine in the tropical troposphere and stratosphere as derived from balloon-borne BrO observations, Atmos. Chem. Phys., 8, 7265–7271, 2008, http://www.atmos-chem-phys.net/8/7265/2008/.

Douglass, A. R. and Kawa, S. R.: Contrast between 1992 and 1997 high-latitude spring Halogen Occultation Experiment observations of lower stratospheric HCl, J. Geophys. Res., 104(D15), 18739–18754, doi:10.1029/1999JD900281, 1999.

Douglass, A. R., Stolarski, R. S., Schoeberl, M. R., Jackman, C. H., Gupta, M. L., Newman, P. A., Nielsen, J. E., and Fleming, E. L.: Relationship of loss, mean age of air and the distribution of CFCs to stratospheric circulation and implications for atmospheric lifetimes, J. Geophys. Res., 113, D14309, doi:10.1029/2007JD009575, 2008.

Dvortsov, V. L., Geller, M. A., Solomon, S., Schauffler, S. M., Atlas, E. L., and Blake, D. R.: Rethinking reactive halogen budgets in the midlatitudes lower stratosphere, Geophys. Res. Lett., 26, 1699–1702, 1999.

Eyring, V., Butchart, N., Waugh, D. W., et al.: Assessment of temperature, trace species, and ozone in chemistry-climate model simulations of the recent past, J. Geophys. Res., 111, D22308, doi:10.1029/2006JD007327, 2006.

Garcia, R. R. and Solomon, S.: A new numerical model of the middle atmosphere: 2. Ozone and related species, J. Geophys. Res., 99, 12937–12951, 1994.

Giorgi, F. and Chameides, W. L.: Rainout lifetimes of highly soluble aerosols and gases as inferred from simulations with a general circulation model, J. Geophys. Res., 91, 14367–14376, 1986.

Goodwin, K. D., Lidstrom, M. E., and Oremland, R. S.: Marine bacterial degradation of brominated methanes, Environ. Sci. Technol., 31, 3188–3192, 1997.

Hoell, J. M., Davis, D. D., Jacob, D. J., Rodgers, M. O., Newell, R. E., Fuelberg, H. E., McNeal, R. J., Raper, J. L., and Bendura, R. J.: Pacific Exploratory Mission in the tropical Pacific:

PEM-Tropics A, August–September 1996, J. Geophys. Res., 104(D5), 5567–5583, 1999.
Hossaini, R., Chipperfield, M. P., Monge-Sanz, B. M., Richards, N. A. D., Atlas, E., and Blake, D. R.: Bromoform and dibromomethane in the tropics: a 3-D model study of chemistry and transport, Atmos. Chem. Phys. Discuss., 9, 16811–16851, 2009, http://www.atmos-chem-phys-discuss.net/9/16811/2009/.
Jacob, D. J., Crawford, J. H., Kleb, M. M., Connors, V. S., Bendura, R. J., Raper, J. L., Sachse, G. W., Gille, J. C., Emmons, L., and Heald, C. L.: Transport and Chemical Evolution over the Pacific (TRACE-P) aircraft mission: Design, execution, and first results, J. Geophys. Res., 108(D20), 9000, doi:10.1029/2002JD003276, 2003.
Jacob, D. J., Crawford, J. H., Maring, H., Clarke, A. D., Dibb, J. E., Ferrare, R. A., Hostetler, C. A., Russell, P. B., Singh, H. B., Thompson, A. M., Shaw, G. E., McCauley, E., Pederson, J. R., and Fisher, J. A.: The ARCTAS aircraft mission: design and execution, Atmos. Chem. Phys. Discuss., 9, 17073–17123, 2009, http://www.atmos-chem-phys-discuss.net/9/17073/2009/.
Klick, S.: The release of volatile halocarbons to seawater by untreated and heavy metal exposed samples of the brown seaweed, *Fucus vesiculosus*, Mar. Chem., 42, 211–221, 1993.
Kroon, M., Petropavlovskikh, I., Shetter ,R., Hall, S., Ullmann, K., Veefkind, J. P., McPeters, R. D., Browell, E. V., and Levelt, P. F.: OMI total ozone column validation with Aura-AVE CAFS observations, J. Geophys. Res., 113, D15S13, doi:10.1029/2007JD008795, 2008.
Kurylo, M. J. and Rodriguez, J. M.: Short-lived ozone related compounds, in: Scientific Assessment of Ozone Depletion: 1998, Global Ozone Res. and Monit. Proj., Rep. 44, chap. 2, World Meteorol. Organ., Geneva, Switzerland, 1999.
Liang, Q., Jaeglé, L., Hudman, R. C., et al.: Summertime influence of Asian pollution in the free troposphere over North America, J. Geophys. Res., 112, D12S11, doi:10.1029/2006JD007919, 2007.
Liang, Q., Stolarski, R. S., Douglass, A. R., Newman, P. A., Nielsen, J. E.: Evaluation of emissions and transport of CFCs using surface observations and their seasonal cycles and the GEOS CCM simulation with emissions-based forcing, J. Geophys. Res., 113, D14302, doi:10.1029/2007JD009617, 2008.
Lin, S.-J.: A "vertically Lagrangian" finite-volume dynamical core for global models, Mon. Weather Rev., 132(10), 2293–2307, 2004.
Livesey, N. J., Kovalenko, L. J., Salawitch, R.,J., MacKenzie, I. A., Chipperfield, M. P., Read, W. G., Jarnot, R. F., and Waters, J. W.: EOS Microwave Limb Sounder observations

of upper stratospheric BrO: Implications for bromine, Geophys. Res. Lett., 33, L20817, doi:10.1029/2006GL026930, 2006.
McElroy, M., Salawitch, R. J., Wolfsy, S., and Logan, J.: Reductions of Antarctic ozone due to synergistic interactions of chlorine and bromine, Nature, 321, 759–762, 1986.
Moorthi, S. and Suarez, M. J.: Relaxed Arakawa–Schubert: A parameterization of moist convection for general circulation models, Mon. Weather Rev., 120, 978–1002, 1992.
Nielsen, J. E. and Douglass A. R.: A simulation of bromoform's contribution to stratospheric bromine, J. Geophys. Res., 106, 8089–8100, 2001.
Ott, L. E., Pawson, S., and Bacmeister, J.: An analysis of the impact of convective arameter sensitivity on simulated global atmospheric CO distributions, Atmos. Chem. Phys. Discuss., in preparation, 2009.
Pawson, S., Stolarski, R. S., Douglass, A. R., Newman, P. A., Nielsen, J. E., Frith, S. M., and Gupta, M. L.: Goddard Earth Observing System Chemistry-Climate Model Simulations of Stratospheric Ozone-Temperature Coupling Between 1950 and 2005, J. Geophys. Res., 113, D12103, doi:10.1029/2007JD009511, 2008.
Quack, B. and Wallace, D. W. R.: Air-sea flux of bromoform: Controls, rates and implications, Global Biogeochem. Cy., 17(1), 1023, doi:10.1029/2002GB001890, 2003.
Raper, J., Kleb, M. M., Jacob, D. J., Davis, D. D., Newell, R. E., Fuelberg, H. E., Bendura, R. J., Hoell, J. M., and McNeal, R. J.: Pacific Exploratory Mission in the Tropical Pacific: PEM-Tropics B, March-April 1999, J. Geophys. Res., 106(D23), 32401–32425, 2001.
Reinecker, M. M., Suarez, M. J., Todling, R., et al.: The GEOS-5 Data Assimilation System-Documentation of Versions 5.0.1, 5.1.0, and 5.2.0, Tech. Rep. 104606 V27, NASA, Greenbelt, MD, 2008.
Schauffler, S. M., Atlas, E. L., Blake, D. R., Flocke, F., Lueb, R. A., Lee-Taylor, J. M., Stroud, V., and Travnicek, W.: Distributions of brominated organic compounds in the troposphere and lower stratosphere, J. Geophys. Res., 104(D17), 21513–21535, 1999.
Singh, H. B., Brune, W. H., Crawford, J. H., Jacob, D. J., and Russell, P. B.: Overview of the summer 2004 Intercontinental Chemical Transport Experiment–North America (INTEX-A), J. Geophys. Res., 111, D24S01, doi:10.1029/2006JD007905, 2006.
Singh, H. B., Brune, W. H., Crawford, J. H., Flocke, F., and Jacob, D. J.: Chemistry and transport of pollution over the Gulf of Mexico and the Pacific: spring 2006 INTEX-B campaign overview and first results, Atmos. Chem. Phys., 9, 2301–2318, 2009, http://www.atmos-chem-phys.net/9/2301/2009/.

ACPD
9, 23623–23664, 2009

Sinnhuber, B.-M., Arlander, D.W., Bovensmann, H., et al.: Comparison of measurements and model calculations of stratospheric bromine monoxide, J. Geophys. Res., 107(D19), 4398, doi:10.1029/2001JD000940, 2002.

Sinnhuber, B.-M., Rozanov, A., Sheode, N., Afe, O. T., Richter, A., Sinnhuber, M., Wittrock, F., Burrows J. P., Stiller, G. P., von Clarmann, T., and Linden ,A.: Global observations of stratospheric bromine monoxide from SCIAMACHY, Geophys. Res. Lett., 32, L20810, doi:10.1029/2005GL023839, 2005.

Sioris, C. E., Kovalenko, L. J., McLinden, C. A., et al.: Latitudinal and vertical distribution of bromine monoxide in the lower stratosphere from Scanning Imaging Absorption Spectrometer for Atmospheric Chartography limb scattering measurements, J. Geophys. Res., 111, D14301, doi:10.1029/2005JD006479, 2006.

Solomon, S., Wuebbles, D., Isaksen, I., Kiehl, J., Lal, M., Simon, P., and Sze, N. D.: Ozone depletion potentials, global warming potentials and future chlorine/bromine loading, in: Scientific Assessment of Ozone Depletion: 1994, Global Ozone Res. and Monit. Proj. Rep. 37, 131–1336, World Meteorol. Organ., Geneva, Switzerland, 1995.

Sturges, W. T., Cota, G. F., and Buckley, P. T.: Bromoform emission from Arctic ice algae, Nature, 358, 6388, 660–662, 1992.

Sturges, W. T., Cota, G. F., and Buckley, P. T.: Vertical profiles of bromoform in snow, sea ice, and seawater in the Canadian Arctic, J. Geophys. Res., 102(C11), 25073–25083, 1997.

Sturges, W. T., Oram, D. E., Carpenter, L. J., Penkett, S. A., and Engel, A.: Bromoform as a source of stratospheric bromine, Geophys. Res. Lett., 27(14), 2081–2084, 2000.

Turquety, S., Logan, J. A., Jacob, D. J., et al.: Inventory of boreal fire emissions for North America in 2004: Importance of peat burning and pyroconvective injection, J. Geophys. Res., 112, D12S03, doi:10.1029/2006JD007281, 2007.

von Glasow, R., von Kuhlmann, R., Lawrence, M. G., Platt, U., and Crutzen, P. J.: Impact of reactive bromine chemistry in the troposphere, Atmos. Chem. Phys., 4, 2481–2497, 2004, http://www.atmos-chem-phys.net/4/2481/2004/.

Yokouchi, Y., Hasebe, F., Fujiwara, M., Takashima, H., Shiotani, M., Nishi, N., Kanaya, Y., Hashimoto, S., Fraser, P., Toom-Sauntry, D., Mukai, H., and Nojiri, Y.: Correlations and emission ratios among bromoform, dibromochloromethane, and dibromomethane in the atmosphere, J. Geophys. Res., 110, D23309, doi:10.1029/2005JD006303, 2005.

Warwick, N. J., Pyle, J. A., Carver, G. D., Yang, X., Savage, N. H., O'Connor, F. M., and Cox, R. A.: Global modeling of biogenic bromocarbons, J. Geophys. Res., 111, D24305,

doi:10.1029/2006JD007264, 2006.
Waugh, D. W., Strahan, S. E., and Newman, P. A.: Sensitivity of stratospheric inorganic chlorine to differences in transport, Atmos. Chem. Phys., 7, 4935–4941, 2007, http://www.atmos-chem-phys.net/7/4935/2007/.
WMO (World Meteorological Organization): Scientific Assessment of Ozone Depletion: 2006, Global Ozone Research and Monitoring Project – Report No. 50, Geneva, Switzerland, 2007.
Yang, X., Cox, R. A., Warwick, N. J., Pyle, J. A., Carver, G. D., and O'Connor F. M.: Tropospheric bromine chemistry and its impacts on ozone: A model study, J. Geophys. Res., 110, D23311, doi:10.1029/2005-JD006244, 2005.

Table 1. Emission distribution of $CHBr_3$ and CH_2Br_2 in Scenario A, B and C.

	Global emissions Gg Br yr^{-1}	Emission distribution					
	$CHBr_3$ (CH_2Br_2)[a]	Open ocean			Coast		
		Latitude	Percentage	Gg Br yr^{-1}[a]	Latitude	Percentage	Gg Br yr^{-1}[a]
Scenario A	425 (57)	50–90° S 10–50° S 10° S–10° N 10–50° N 50–90° N	1.1% 11.1% 33.3% 13.3% 1.1%	5 (1) 47 (6) 141 (20) 57 (20) 5 (1)	50–90° S 10–50° S 10° S–10° N 10–50° N 50–90° N	1.1% 11.1% 4.4% 22.2% 1.1%	5 (1) 47 (6) 19 (3) 94 (13) 5 (1)
Scenario B	380 (104)	20° S–20° N 20–50° S/N	75% 25%	285 (78) 95 (26)		None	
Scenario C	565 (57)	20° S–20° N 20–50° S/N	37.8% 6.3%	214 (21) 71 (7)	10° S–10° N	49.6%	280 (29)

[a] Emissions of CH_2Br_2 are in the parentheses.

ACPD
9, 23623–23664, 2009

Table 2. A summary of aircraft observations used in this study.

	Missions	Time	Area	References
PEM-Tropics[1]	PEM-Tropics A PEM-Tropics B	August–October 1996 March–April 1999	75° S–50° N, 150° E–100° W 40° S–40° N, 140° E–70° W	Hoell et al. (1999) Raper et al. (2001)
TRACE-P[2]		February–April 2001	10–40° N, 140° E–80° W	Jacob et al. (2003)
INTEX[3]	INTEX-A INTEX-B	July–August 2004 March–May 2006	10–45° N, 70–130° W 15–70° N, 170° E–90° W	Singh et al. (2006) Singh et al. (2009)
TC4[4]		July–August 2007	10° S–40° N, 60–130° W	
ARCTAS[5]	ARCTAS-A ARCTAS-B	April 2008 June–July 2008	30–90° N, 20° E–50° W 30–90° N, 20–140° W	Jacob et al. (2009) Jacob et al. (2009)
STRAT[6]		January–December 1996	0–10° N, 0–140° W	Schauffler et al. (1999)
Pre-AVE[7]		January–February 2004	10° S–40° N, 80–100° W	
AVE[8]	HAVE-2 CRAVE	June 2005 January–February 2006	10–90° N, 100° W–30° E 0–40° N, 80–100° W	Kroon et al. (2008) Kroon et al. (2008)

[1] The Pacific Exploratory Missions – Tropics (PEM-Tropics) mission.
[2] The Transport and Chemical Evolution over the Pacific (TRACE-P) mission.
[3] The Intercontinental Chemical Transport Experiment (INTEX) mission.
[4] The Tropical Composition, Cloud and Climate Coupling (TC4) mission.
[5] The Arctic Research of the Composition of the Troposphere from Aircraft and Satellites (ARCTAS) mission.
[6] The Stratospheric Tracers of Atmospheric Transport (STRAT) mission.
[7] The Pre-Aura Validation Experiment (Pre-AVE).
[8] The Aura Validation Experiment (AVE). Data from two AVE campaigns are used in this study: i) 2005 June Houston AVE (HAVE-2) campaign, ii) 2006 January Costa Rica AVE (CRAVE) campaign.

ACPD
9, 23623–23664, 2009

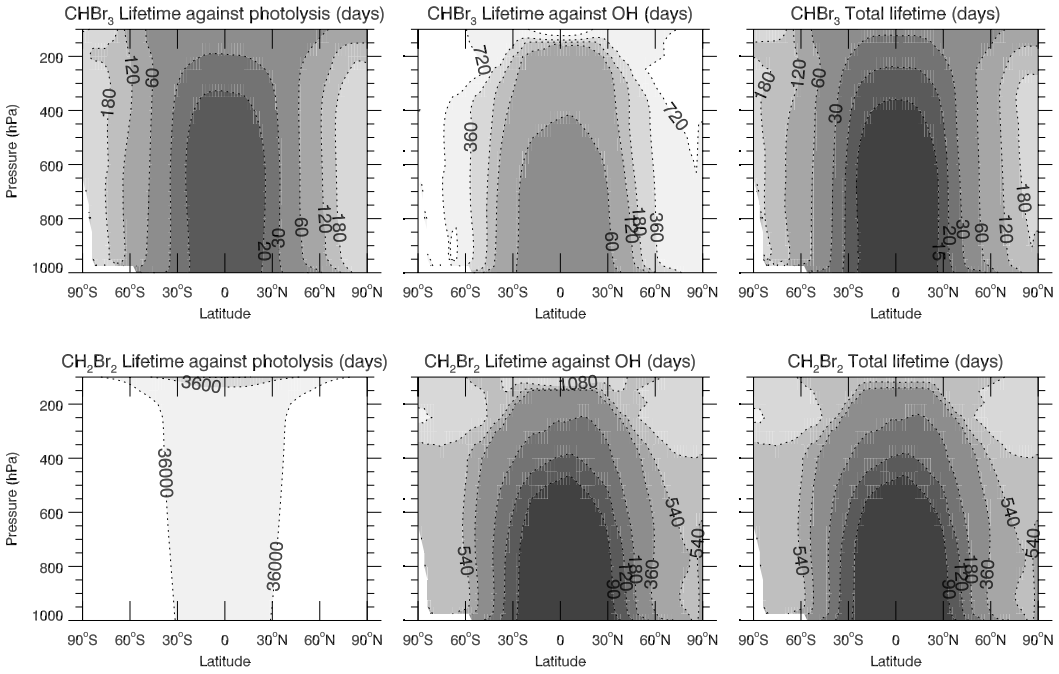

Fig. 1. Model calculated local lifetime of $CHBr_3$ and CH_2Br_2 against photolysis, reaction with OH, and total lifetime.

ACPD
9, 23623–23664, 2009

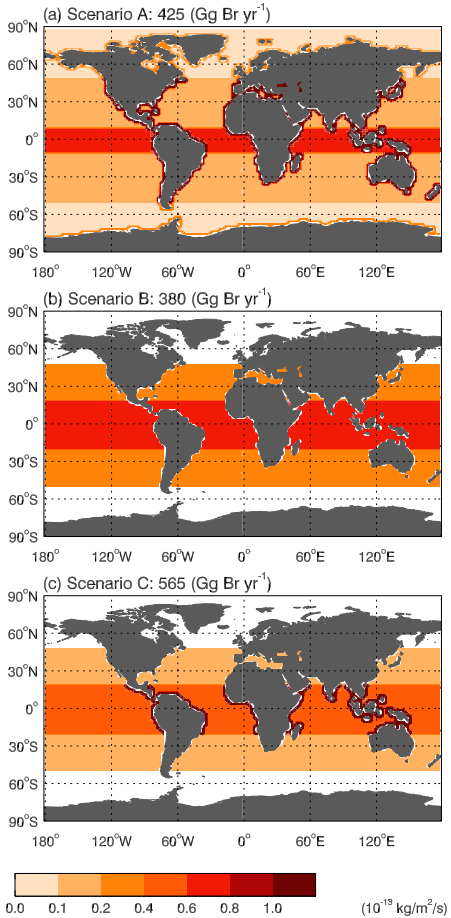

Fig. 2. Global emission distribution for $CHBr_3$ in **(a)** Scenario A, **(b)** Scenario B, and **(c)** Scenario C.

ACPD
9, 23623–23664, 2009

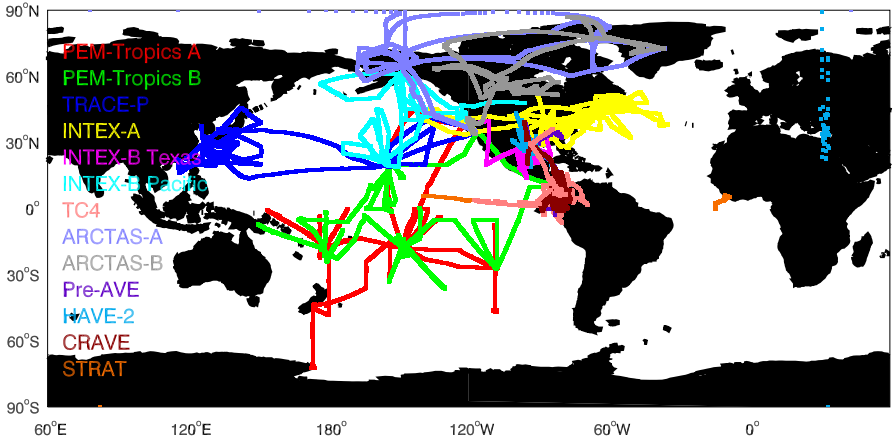

Fig. 3. Flight tracks for aircraft missions used in this study (Table 2).

ACPD
9, 23623–23664, 2009

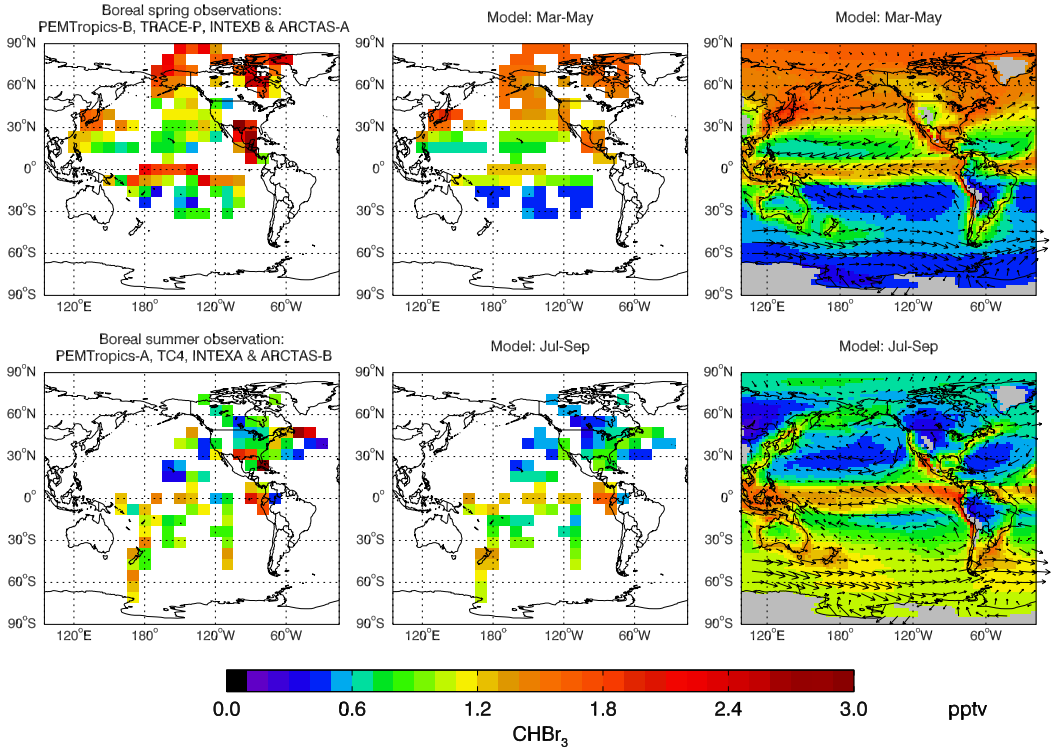

Fig. 4. Left column: the composite of airborne observations of $CHBr_3$ in the lower troposphere (1000–800 hPa) during boreal spring and summer. Middle column: the simulated 1000–800 hPa mean $CHBr_3$ between March-May (upper panel) and July–September (lower panel), sampled at the same location as the observations. Right column: same as the middle column but for the entire Pacific/North American region. The model results are from the simulation run with emission scenario A.

ACPD
9, 23623–23664, 2009

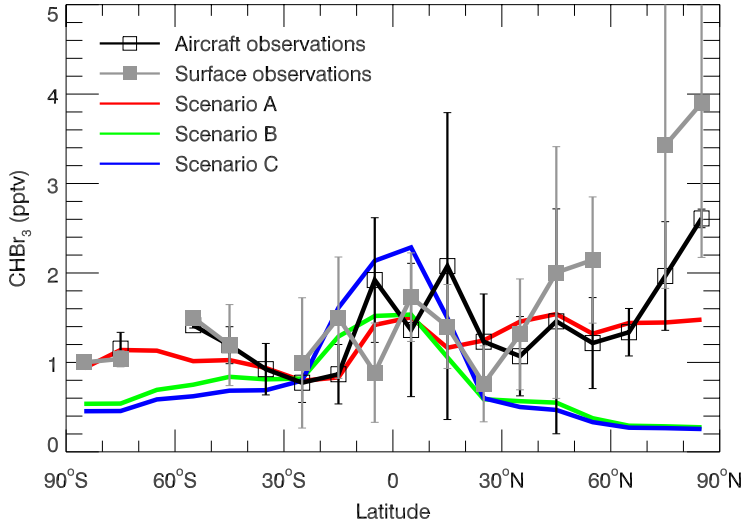

Fig. 5. Latitudinal dependence of $CHBr_3$ at the surface. Black line (open squares indicate mean and vertical error bar indicate one standard deviation) shows aircraft observations averaged below 1 km and averaged for each 10° latitude band. Surface measurements from Table 2 in Quack and Wallace (2003) are plotted in gray line with filled squares. The simulated zonal averaged $CHBr_3$ between 0–1 km are plotted in color. We use consistent colored lines for model results from different simulations for this figure, Figs. 6, 7, 9, and 10: simulations with emission scenario A in red, scenario B in green, and scenario C in blue.

ACPD
9, 23623–23664, 2009

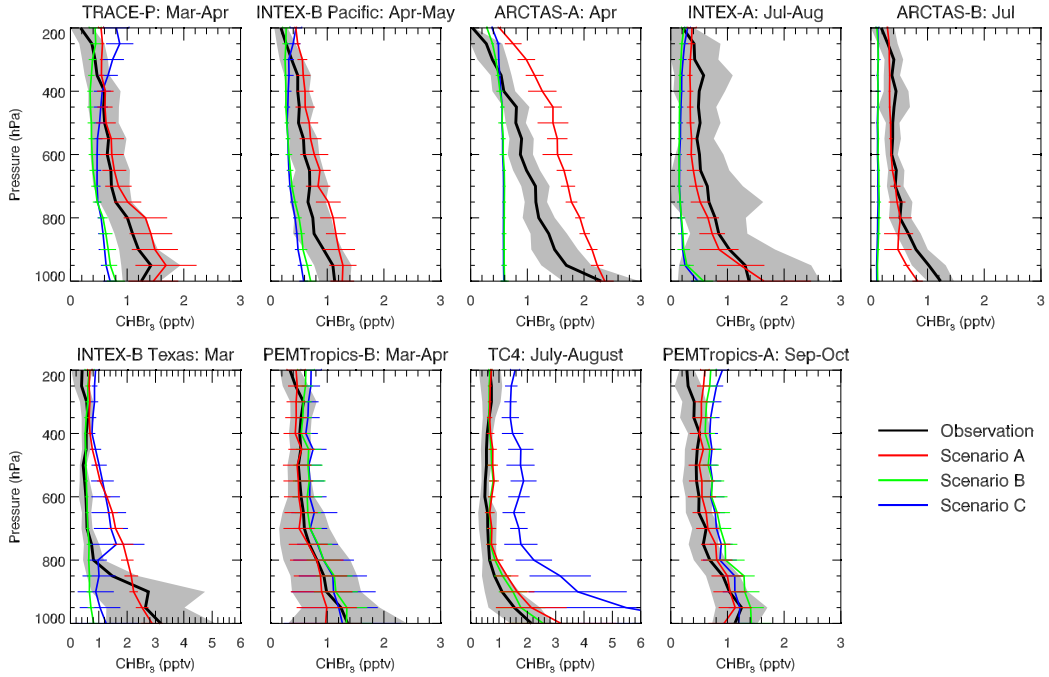

Fig. 6. Comparison of the observed and simulated vertical profiles of $CHBr_3$ in the troposphere during individual aircraft missions. The upper row shows missions that took place in the northern mid and high latitudes and the lower row shows those in the tropics and southern hemisphere. Black lines show the observed mean concentrations with one standard deviation marked by gray shading. The mean CH_2Br_2 vertical profiles from three simulations are plotted in color with horizontal bars indicate one standard deviation. Model is sampled at the same location as the observations in the corresponding month.

ACPD
9, 23623–23664, 2009

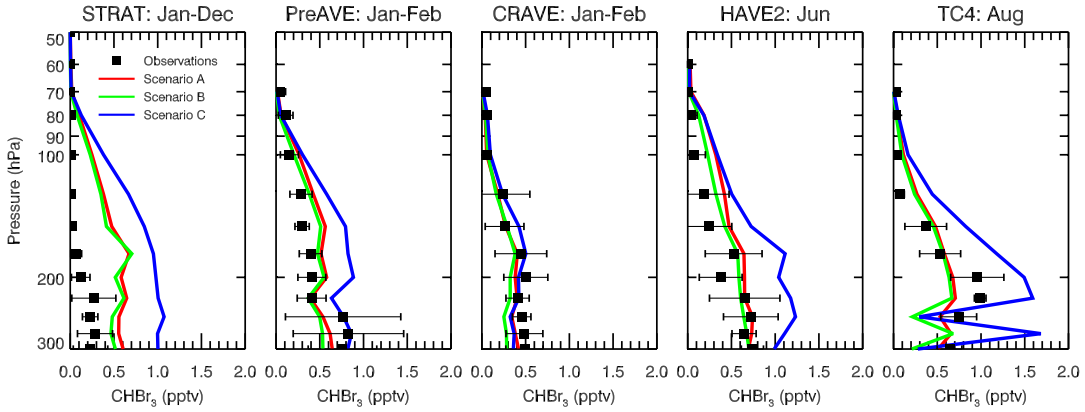

Fig. 7. Similar to Fig. 6 but for the UT/LS region.

ACPD
9, 23623–23664, 2009

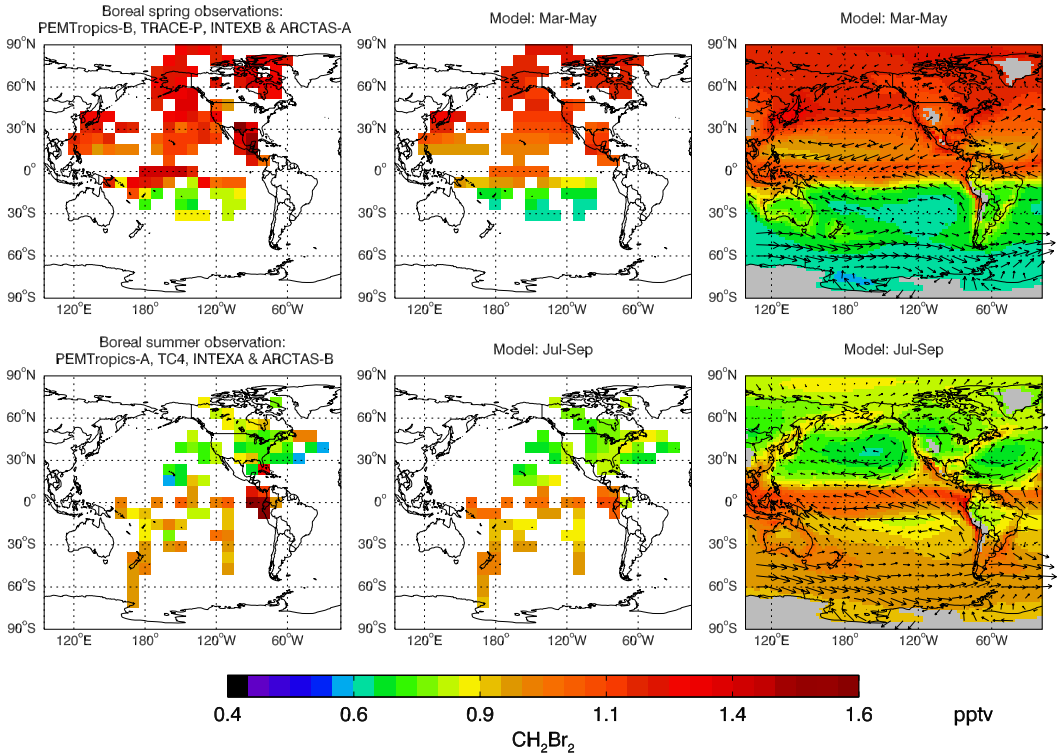

Fig. 8. Same as Fig. 4 but for CH_2Br_2.

ACPD
9, 23623–23664, 2009

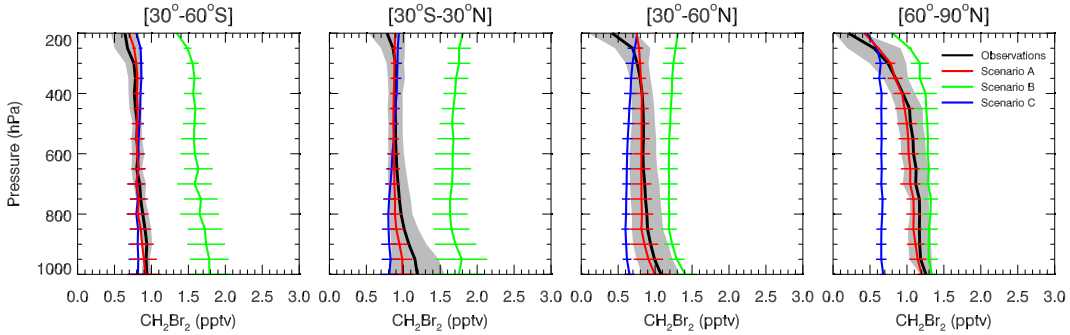

Fig. 9. Comparison between the observed and simulated vertical profiles of CH_2Br_2 in the troposphere. Observations from all available aircraft missions are averaged for 30–60° S, 30° S–30° N, 30–60° N, and 60–90° N latitude bands at 1-km vertical interval. Black lines show the mean concentrations with gray shadings indicate one standard deviation. The mean CH_2Br_2 vertical profiles from three simulations are plotted in color with horizontal bars indicate one standard deviation. Model is sampled at the same location as the observations in the corresponding month.

ACPD
9, 23623–23664, 2009

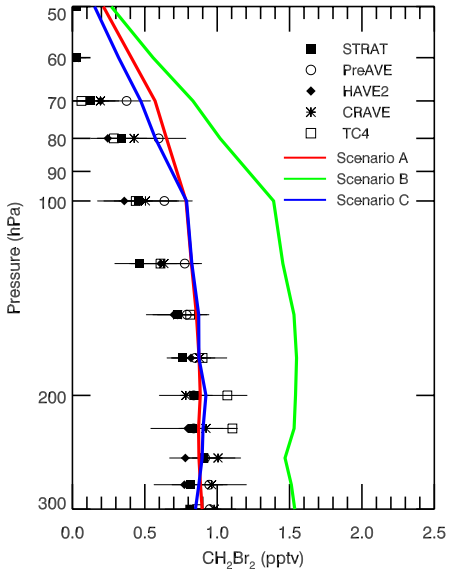

Fig. 10. Comparison between the observed and simulated vertical profiles of CH_2Br_2 in the UT/LS. Observations from the Pre-AVE (open circle), HAVE2 (filler diamond), CRAVE (asterisk), and TC4 (open square) missions are shown. Error bar indicates one standard deviation. The mean CH_2Br_2vertical profiles from three simulations are plotted in color. Model is sampled at the same location as the observations in the corresponding month.

ACPD
9, 23623–23664, 2009

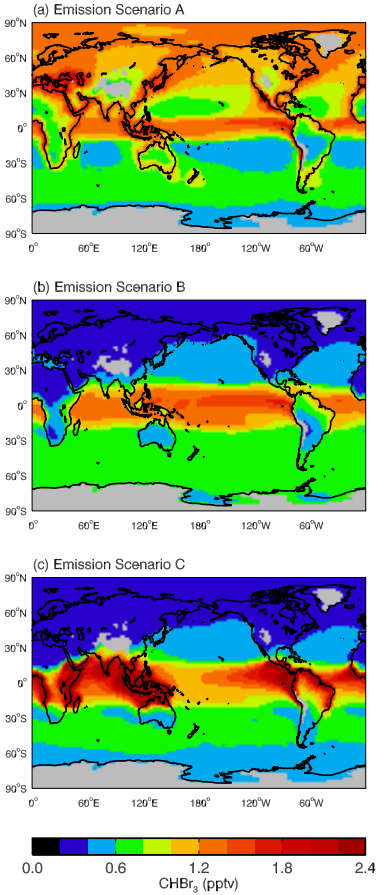

Fig. 11. The annual mean horizontal distribution of $CHBr_3$ in the lower troposphere (1000–800 hPa) from simulations conducted with emission **(a)** Scenario A, **(b)** Scenario B, and **(c)** Scenario C.

ACPD
9, 23623–23664, 2009

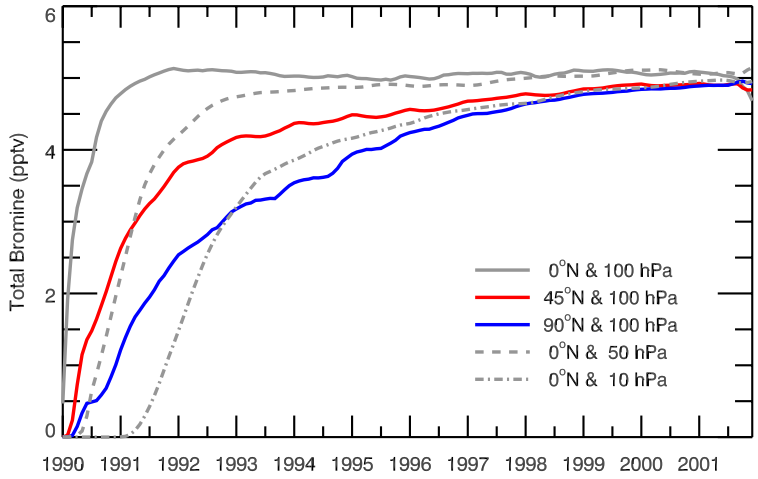

Fig. 12. Simulated total bromine at 100 hPa (gray solid line), 50 hPa (gray dashed line), and 10 hPa (gray dash-dotted line) at the equator, as well as those at 45° N (red) and 90° N (blue) at 100 hpa between January 1990 and December 2001. We apply a 13-month running mean filter to each monthly-mean time series to remove seasonal variations.

ACPD
9, 23623–23664, 2009

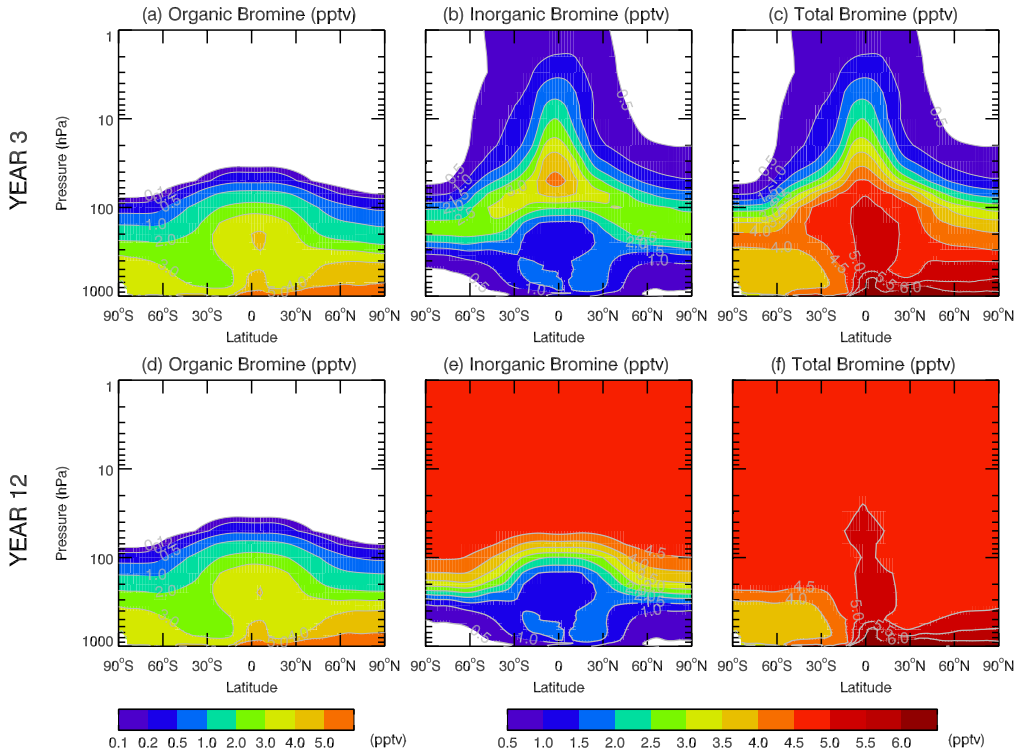

Fig. 13. The latitude-pressure cross section of the contribution of $CHBr_3$ and CH_2Br_2 to organic bromine (left column), inorganic bromine (middle column) and total bromine (right column) from year 3 and year 12 of the simulation.

ACPD
9, 23623–23664, 2009

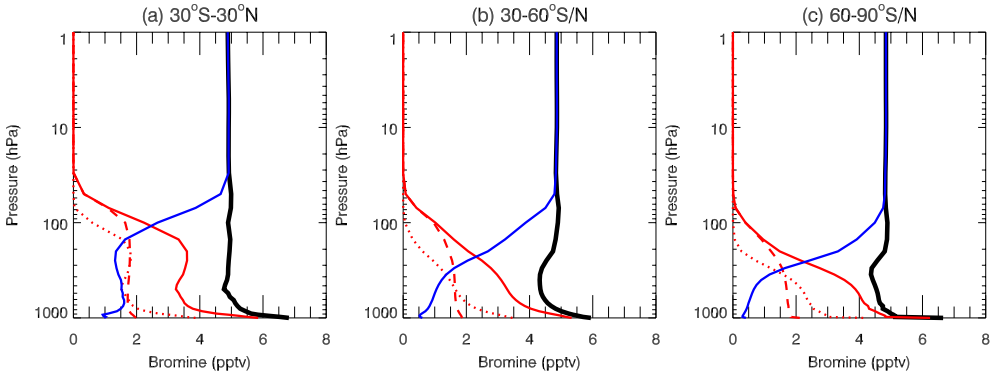

Fig. 14. The model calculated contribution of organic bromine (red solid lines), inorganic bromine (blue lines), and total bromine (black lines) from short-lived bromocarbons at steady state, averaged between **(a)** 30° S–30° N, **(b)** 30–60° S/N, and **(c)** 60–90° S/N. The relative contribution of bromine from $CHBr_3$ ($CHBr_3 \times 3$, red dotted lines) and CH_2Br_2 ($CH_2Br_2 \times 2$, red dashed lines) to organic bromine is also included.

ACPD
9, 23623–23664, 2009